One-pot hydrothermal synthesis of ZnO-reduced graphene oxide composites using Zn powders for enhanced photocatalysis

Shizhen Liu[1], Hongqi Sun[1], Alexandra Suvorova[2], Shaobin Wang[1]*

[1]*Department of Chemical Engineering, Curtin University, GPO Box U1987, Perth, WA 6845, Australia*

[2]*Centre for Microscopy, Characterisation and Analysis, The University of Western Australia, Crawley, WA 6009, Australia*

(*) Corresponding author: shaobin.wang@curtin.edu.au; Tel: +61 8 93663776; Fax: +61 8 92662681

Abstract

Zn powder was successfully utilized as a reducing agent and a precursor of ZnO for one-pot synthesis of reduced graphene oxide (rGO)-ZnO photocatalysts. Two rGO-ZnO composites were synthesized with or without a surfactant, cetyltrimethyl ammonium bromide (CTAB). The structural, morphological, and photochemical properties of the samples were thoroughly investigated by X-ray diffraction (XRD), Fourier transform infrared spectroscopy (FT-IR), field emission scanning electron microscopy (FE-SEM), transmission electron microscopy (TEM), N_2 adsorption/desorption, UV-vis diffuse reflectance (UV-vis DRS), thermogravimetric-differential thermal analysis (TG-DTA), and Raman spectroscopy. Zn powder could effectively reduce GO to graphene and be transformed to ZnO with the assistance of the surfactant. The surfactant was found to influence the properties of rGO-ZnO. rGO-ZnO photocatalysts could decompose methylene blue under UV-vis illumination and exhibited higher activities than pristine ZnO. The co-existence of GO-rGO would be more favorable to photocatalysis.

Key words: ZnO; reduced graphene oxide; methylene blue; photocatalysis

1. Introduction

Graphene as a novel carbonaceous nanomaterial is a single- or multiple-layer carbon atom sheet with two dimensional aromatic structure, which has good Young's modulus (~1100 GPa), fracture strength (125 GPa), thermal conductivity (~5000 $Wm^{-1}K^{-1}$), specific surface area (theoretical value of 2630 m^2g^{-1}), magnetism and fascinating transport properties [1]. Those remarkable characteristics of graphene have stimulated worldwide interests in its experimental and theoretical investigations as well as other novel applications [1-5]. Currently, the methods for a large scale production of graphene have been established based on chemical reduction of graphene oxide (GO) using different chemicals such as hydrazine [6], dimethylhydrazine, sodium borohydride or strong alkaline solutions (NaOH, KOH, NH_4OH with pH value higher than 10) [7]. Obviously these chemical reagents are toxic or harmful to the environment or human health. Wu et al. demonstrated that high-quality graphene could be obtained by vacuum reduction of GO at around 1000 °C in H_2 gas. However, this method consumed the carbonaceous material at high temperature [8]. This process was later used as an efficient method to synthesize graphene sheets in a large scale [9], but the quality of reduced GO (rGO) was strongly relied on the experimental conditions [10].

Semiconductors like TiO_2 are widely used in photocatalysis, however, they often have to be modified by transition metals, noble metals, or non-metal elements to improve optical property and electron transfer process [11, 12]. In this way, the light absorption will be extended to visible light range and the electron-hole recombination will be suppressed to enhance the photocatalytic activity. The dopants can also improve the stabilization of photocatalyst surface [1]. Zinc oxide as another important semiconductor material can only absorb ultraviolet (UV) light to yield photoelectrons and holes to effectively degrade organic pollutants [13-15], similar to TiO_2, and it sometimes shows a higher photocatalytic activity than TiO_2 [16, 17].

Currently, rGO functionalized ZnO has been synthesized for photocatalysis because rGO possesses the ability to accept electrons, and favors adsorption of aromatic compounds due to π-π conjunction [18]. Most of previous investigations employed zinc salts or commercial zinc oxide nanocrystals for hydrothermal deposition of ZnO on rGO sheets [13, 14, 16, 19-22]. It is known that graphene is poorly soluble in water and polar organic solvents and easily aggregates owing to strong van der Waals force. The hydrophobic/hydrophilic incompatibility between graphene and inorganic compounds (especially metal oxides) also

makes it difficult to directly deposit metal oxides on graphene. Thus a dispersant is usually needed to help metal oxides be attached to graphene [22, 23].

Fan et al. recently reported the use of iron powder for reduction of graphene oxide in acid solution [23]. Mei and Ouyang have made rGO by zinc powder in HCl solution with ultrasonics [9]. Another research indicated that metal assisted GO reduction is more effective than other reduction processes [24]. In addition, hydrothermal method helps to obtaining ZnO particles with a narrow size distribution, less defect crystallization, no particle agglomeration and more phase homogeneity [25, 26]. Thus, using Zn metal in hydrothermal synthesis without any toxic and harmful chemicals like hydrazine or $NaBH_4$ to get ZnO-graphene photocatalyst will be a new and promising method.

Herein we present a one-pot hydrothermal approach to prepare rGO-ZnO composites using Zn powder with a cationic surfactant, cetyltrimethyl ammonium bromide (CTAB) or without the surfactant. Zn powder will be a ZnO precursor and a reducing agent for GO. The rGO-ZnO photocatalysts were then tested for photodegradation of methylene blue (MB) as a water organic pollutant under ultraviolet and visible radiation (UV-vis light). It was found that synthesis of rGO-ZnO composites could be achieved using Zn powder and GO as precursors. More importantly, rGO-ZnO exhibited enhanced photocatalytic performance as compared with naked ZnO.

2. Experimental

2.1 Materials and reagents

Graphite powder (purity 99.9995%), sulphuric acid (95–97%), and cetyltrimethyl ammonium bromide (CTAB) were obtained from Sigma–Aldrich Chemical Corporation. Hydrogen peroxide (30%) was purchased from Chem-Supply. Methylene blue (MB), potassium permanganate, and hydrochloric acid (32%, analytical grade) were obtained from Biolab. Zinc powder was obtained from the Australian Metal Powders Supplies.

2.2 Synthesis of rGO-ZnO photocatalysts

Graphene oxide (GO) was prepared by the Hummers method [27, 28]. Then GO was dispersed in aqueous solution (0.0112 g/mL) with ultrasonics for 2 h. Two rGO-ZnO samples were then prepared by a one-pot hydrothermal method. In a typical synthesis, 2 g zinc powders were mixed with 40 mL GO suspension (pH = 2.2), then CTAB powder was gradually added into the solution until its final concentration at 0.1 M. The solution was

magnetically stirred for 2 h and transferred into a Teflon-lined stainless steel autoclave (80 mL). Hydrothermal reaction was carried out at 195 °C for 24 h. Black sediment was collected and cleaned with ethanol and distilling water several times and then dried in air at 60 °C. This is referred to as G-ZnO-CTAB. The diagram of G-ZnO-CTAB formation is presented in Fig.1. The other G-ZnO sample was synthesized in the same way without addition of CTAB. In addition, a pristine ZnO was also prepared without using GO. For a comparison, another G-ZnO composite using $ZnCl_2$ salt as a ZnO precursor was also synthesized. For this, GO solution and $ZnCl_2$ were mixed and solution pH was adjusted to 10 using KOH. Then the liquid was put in a 120 mL autoclave at 195 ºC for 24 h. After that, the solid was collected, washed, and calcined at 350 ºC for 1 h in N_2. This sample was referred as G-ZnO-350. For G-ZnO-CTAB, different GO concentrations were also used for preparation to investigate the effect of GO loading.

For ZnO formation under hydrothermal condition, it is believed that active Zn atoms located at the surface of zinc particle react with water first at low pH. As a result, the concentration of zinc ions and OH^- around the zinc particles increases. $Zn(OH)_2$ is then formed in situ via the reaction between Zn^{2+} and OH^-. Under hydrothermal condition, $Zn(OH)_2$ can dehydrate to produce ZnO [26]. The formation process can be shown as below.

$$Zn + 2\ H_2O \rightarrow Zn^{2+} + H_2 \uparrow + 2\ OH^- \quad (1)$$

$$Zn^{2+} + 2\ OH^- \rightarrow Zn(OH)_2 \rightarrow ZnO + H_2O \quad (2)$$

The possible processes for ZnO nanoparticle formation on GO under hydrothermal conditions can be represented as follows:

$$Zn + GO_xH_y \rightarrow Zn^{2+} + y/2\ H_2 + GO_x^{y-} \quad (3)$$

$$Zn^{2+} + GO^{z-} + OH^- \rightarrow (GOZn)^{z+}z(OH)^- + Zn(OH)_4^{2-} \rightarrow G(ZnO) + ZnO + H_2O \quad (4)$$

Fig.1

2.3 Characterization of materials

UV–visible diffuse reflectance spectra (UV-vis DRS) of samples were recorded on a JASCO V-670 spectrophotometer with an Ø 60 mm integrating sphere, and $BaSO_4$ was used as a reference material. The crystalline structure of samples was analyzed by powder X-ray

diffraction (XRD) using a Bruker D8-Advance X-Ray diffractometer with Cu Kα radiation (λ = 1.5418 Å). Field emission scanning electron microscopy (FE-SEM), performed on a Zeiss Neon 40EsB spectrometer, was used to evaluate the morphology, size and texture information of the samples. Raman spectra were recorded on a Dilor Labram 1B dispersive Raman spectrometer by adopting a laser of 633 nm as incident light. TGA analyses were conducted on a TGA/DSC-1 thermogravimetric analyzer supplied by the Mettler-Toledo Instrument. The textural properties of specific surface area (SSA) and pore volume were obtained from N_2 adsorption analysis at −196 ºC by using a TriStar II 3020. All samples were degassed at 80 ºC for 12 h prior to the analysis. The SSA and pore volume were obtained by the BET equation and adsorption at $p/p^0 = 0.95$, respectively. Transmission electron microscopy (TEM) was carried out using a JEOL 3000 F field emission TEM equipped with a digital camera and Oxford instrument EDS system at 300 kV.

2.4 Photocatalytic tests of ZnO and rGO-ZnO composites

Photocatalytic activities of ZnO and rGO-ZnO samples were evaluated by decomposition of methylene blue under ultraviolet and visible light irradiations. A MSR 575/2 metal halide lamp (575 W, Philips) was utilized as a radiation source. The average intensities of the lamp were measured to be 21.31 $\mu W/cm^2$, 6.941×10^3 $\mu W/cm^2$, and 129.6×10^3 $\mu W/cm^2$ at wavelengths of 220-280 nm, 315-400 nm and 400-1050 nm, respectively. In a typical process, 200 mL, 10 mg/L methylene blue (MB) solution with 0.05 g photocatalyst was continuously stirred in a 1000 mL double-jacket cylindrical Pyrex vessel reactor, which was placed 20 cm away from light source and irradiated under UV-visible light without a filter. The reaction temperature was controlled by recycled cooling water at 25 °C in a water bath. Concentration of methylene blue was measured by the absorption spectroscopic technique. In a regular interval, 4 mL aliquots were taken from the reactor and separated from catalyst particles in a centrifuge at 4700 rpm for 10 min and the absorbance was determined at λ=664 nm with a UV-visible spectrophotometer.

3. Results and discussion

Fig.2 shows XRD patterns of G-ZnO, G-ZnO-CTAB and GO. G-ZnO and G-ZnO-CTAB demonstrated different patterns. GO showed a typical peak at 2θ of 11°, corresponding to the (002) reflection of carbon. The peak at 2θ of 43° is referred to GO (100) reflection. The

reflections of ZnO in a hexagonal wurtzite lattice (JCPDS 75-0576, a =0.3249 nm, c=0.5205 nm) were observed [26, 29] on both G-ZnO and G-ZnO-CTAB composites, indicating that ZnO particles attached onto rGO were highly crystalline. In addition, no (002) peak of graphene oxide could be observed at 2θ between 10 to 15° in G-ZnO-CTAB sample, suggesting that GO has been reduced to graphene. No strong graphene reflection appeared because CTAB is able to effectively exfoliate graphene sheets and prevent their agglomeration [30]. However, (002) diffraction of GO was observed on G-ZnO and the position showed a shift to 12°. It suggests that GO could not be fully reduced to graphene without CTAB and there is a strong interaction between ZnO crystallites and graphene oxide [31]. Previous investigations have found that CTAB can also be a reductant in hydrothermal process. Without CTAB, GO reaction rate with Zn powder will be significantly low, resulting in partial reduction of GO.

Fig.2

FTIR spectra of GO, G-ZnO and G-ZnO-CTAB are presented in Fig.3. For GO, strong O–H stretching at 3600 cm^{-1}, C-O stretching at 1060 cm^{-1}, and C-OH stretching at 1160 cm^{-1} were clearly observed, suggesting the presence of hydroxyl, carboxyl and oxygenate functional groups. The G-ZnO and G-ZnO-CTAB have similar FTIR profiles. For G-ZnO and G-ZnO-CTAB samples, the bands associated with the oxygen functional groups were mostly eliminated. However, G-ZnO and G-ZnO-CTAB still has a stretching peak at 1060 cm^{-1}, which indicates a stronger Zn-O-C combination. The weak peaks at 2930 and 2852 cm^{-1} are also observed on G-ZnO-CTAB due to the stretching vibration of C–H bonds. The introduction of the acidic environment and CTAB can improve the reduction potential of metal to produce rGO [23].

Fig.3

Raman spectroscopy is widely used to study the ordered/disordered crystalline structures of carbonaceous materials. Fig.4 showed the Raman spectra of GO, ZnO, G-ZnO-CTAB, and G-ZnO. The D and G bands arise at 1325 cm^{-1} and 1580 cm^{-1}, respectively on GO [32]. The tiny dislocation of G band of G-ZnO and G-ZnO-CTAB samples suggested more defects and heteroatom implanting. The increasing of peak intensity ratio of I_D/I_G for G-ZnO and G-ZnO-CTAB indicated a decline in the average size of the sp^2 domains [33] and more defects being created [34-36]. The similar 2D peaks of ZnO containing samples indicate that the graphene stack structure has not been changed with or without CTAB [37]. However, G-ZnO presented

strong Raman peaks of ZnO while the peaks on G-ZnO-CTAB were relative weak, indicating that more ZnO particles are strongly attached to GO surface for G-ZnO. During hydrothermal synthesis of G-ZnO-CTAB, CTAB as a cationic ion can interact with growth units of ZnO, covering Zn surface. Due to negative charge of graphene oxide surface, CTAB-Zn particles can not be strongly attracted to GO surface, preventing the formation of G-ZnO composites, but unattached ZnO. XRD results (Fig.2) showed the higher intensity of ZnO crystallites on G-ZnO-CTAB, which suggests more separated ZnO particles on the sample. Fig.S1 shows TEM images of ZnO and ZnO on graphene. As seen ZnO particles are presented either as separated or anchored particles on graphene with particle size around 100 - 200 nm. The EDS analysis has confirmed that the nanoparticles are composed from Zn and oxygen.

Fig.4

TGA is a widely used method to characterize particle thermal stability. Fig.5 reveals TG-DTA curves of GO, G-ZnO and G-ZnO-CTAB. For GO, TG curve exhibited two-step weight loss. The first one was due to the removal of oxygen-containing groups, which is accompanied by the liberation of CO_X and H_2O species at about 120 ºC [6]. The second step was owing to combustion of carbon structure, confirmed by a sharp exothermic peak at 580 ºC in DTA curve. In the curves of G-ZnO and G-ZnO-CTAB, there is about 20% weight loss in total and there are two mass-loss steps at different temperatures. The second weight loss on G-ZnO-CTAB occurred at higher temperature than that on GO and G-ZnO. The DTA curve of G-ZnO-CTAB did not demonstrate an exothermic peak at about 580 ºC, which appeared in the profile of GO and G-ZnO. This is attributed to the higher extent of GO reduction on G-ZnO-CTAB than G-ZnO. XRD analysis shows the presence of GO on G-ZnO, which will decompose at low temperature as bulk GO.

Fig.5

Fig.6A reveals UV-vis diffuse reflectance spectra of synthesized ZnO and rGO-ZnO samples. All samples have a strong absorption edge before 400 nm. ZnO showed gradually reduced absorption in visible-light region while other two rGO-ZnO samples demonstrated strong and stable absorption in the visible region. The curves of $(\alpha h\upsilon)^2$ versus $h\upsilon$ (Fig.6B) for band gap calculation indicated that the band gap of three samples did not change significantly. The band gap of pristine ZnO is 3.07 eV. In contrast, rGO-ZnO photocatalysts exhibited smaller band gap energy. The band gap energies for G-ZnO-CTAB and G-ZnO are 3.03 and 2.96 eV, respectively.

Fig.6

The band-gap energy of ZnO was not reduced significantly by graphene because of rGO-ZnO interposed structure [14], which restricts the interaction of ZnO and graphene. Several previous investigations [14, 16, 22, 38] have reported that ZnO and rGO-ZnO particles have similar absorption edge. It is also accepted that graphene sheet will enhance visible light absorption but weak absorption in ultraviolet light [39].

Fig. 7 shows SEM images of ZnO, G-ZnO and G-ZnO-CTAB. Fig.7 (A, B) shows that most of pristine ZnO particles presented in hexagon with a particle size at 200 nm. Few larger particles were also found. However, ZnO morphology was different on rGO-ZnO samples (Fig.7 C, D, E, F). Obviously, many layers of graphene sheets can be found in rGO-ZnO samples, because GO could be well dispersed in aqueous solution of CTAB [40]. For G-ZnO and G-ZnO-CTAB, ZnO nanoparticles were anchored onto the surface of rGO sheets and they were intercalated between the graphene "Sandwich" aggregations. There are some hexagonal ZnO particles appeared in G-ZnO-CTAB (Fig.7E, F), which means CTAB can effectively promote ZnO growth on graphene sheets.

Fig.7

N_2 adsorption/desorption isotherms of G-ZnO and G-ZnO-CTAB are presented in Fig. S2. Both samples showed similar N_2 isotherm profiles with a hysteresis loop at p/p_0 at 0.5. The BET surface area and pore volume of G-ZnO are 7.3 m^2/g and 0.025 cm^3/g, respectively. For G-ZnO-CTAB, BET surface area and pore volume are similar at 7.4 m^2/g and 0.026 cm^3/g, respectively.

Graphene-ZnO nanoparticles were tested for MB degradation under UV-visible illumination (Fig.8). Zinc oxide demonstrated no MB adsorption but it showed activity in MB degradation. About 98% MB degradation was achieved in 4 h. Meanwhile, G-ZnO, G-ZnO-CTAB and G-ZnO-350 showed adsorption of MB due to the presence of graphene and GO sheets. G-ZnO presented higher adsorption owing to a higher GO content than G-ZnO-CTAB. G-ZnO-350 presented the highest MB adsorption at 20%. It has been found that GO exhibited high MB adsorption [41]. In photocatalytic degradation of MB, G-ZnO, G-ZnO-CTAB and G-ZnO-350 showed a much higher rate in MB decomposition than pristine ZnO. MB degradation at 100% would take 90 min on G-ZnO catalyst, and G-ZnO-CTAB could decompose MB at 100% in 150 min. G-ZnO-350 presented slightly low activity than G-ZnO. We have prepared two graphene modified TiO_2 catalysts using commercial P25 (G-P25) and titanium isopropoxide

(G-TiO_2) with CTAB by a hydrothermal method for MB degradation [12]. Under the similar conditions, G-P25 presented lower overall decolouration of MB at 100% in 80 min and G-TiO_2 was able to degrade MB at 100% in 110 min. In addition, G-Ta_2O_5 was also tested in photocatalytic MB degradation to show 72.1% MB degradation in 120 min [42]. Therefore, it is seen that G-ZnO presented better activity than G-TiO_2 and G-Ta_2O_5.

It has been reported that the photoexcited TiO_2 and ZnO particles are capable of transferring electrons to graphene oxide readily and reduced graphene oxide is capable of storing electrons and transporting them to the catalytic sites to reduce metal ions [43]. Xu et al. [16] tested photocatalytic performance of ZnO via graphene hybridization and found that graphene hybridized ZnO photocatalysts showed enhanced photocatalytic activity for the degradation of organic dyes, which was attributed to the high migration efficiency of photo-induced electrons and the inhibited charge carriers recombination. Fan et al. [44] also synthesized a series of ZnO and graphene composites, which exhibited enhanced photocatalytic performance for degradation of MB due to the efficient charge transfer process. Li and Cao [45] reported that a ZnO@graphene composite exhibited enhanced performance for photocatalytic degradation and filtered removal of rhodamine B dye due to efficient photosensitized electron injection and slow electron recombination.

In this investigation, two rGO-ZnO composites from Zn powder were prepared. SEM images clearly show ZnO deposition on graphene sheets. UV-vis DRS also presents the strong absorption of the two composites in visible range and lower band gap energy for the two composites. In MB photocatalytic degradation, rGO-ZnO will absorb more light to produce electrons from ZnO. The stimulated electrons will quickly transfer to graphene surface due to its high conductivity and attack MB adsorbed on graphene surface or induce $^{\bullet}OH$, preventing the recombination and making the two rGO-ZnO composites exhibiting higher MB degradation than pure ZnO.

XRD and TGA analyses indicated that GO was partially reduced to graphene for G-ZnO. Adsorption tests also showed higher adsorption of MB on G-ZnO. Raman spectra indicated stronger signal of ZnO on G-ZnO surface. In addition, G-ZnO has lower band gap energy than G-ZnO-CTAB. It has been proposed that the conduction band of ZnO is at -4.05 eV and valence band is at -7.25 eV. GO is a semiconductor with a work function energy at -4.42 eV [46]. Such an energy level of GO is helpful to photo electrons transmission from ZnO to GO, reducing the recombination of electronic pairs. Thus in the process of photocatalytic MB degradation on G-ZnO, radiation energy stimulates the electrons from ZnO and the presence

of mixed phases of GO and rGO will promote transferring electrons from photoexcited ZnO to graphene oxide and storing of electrons on graphene and migrating to MB on G-ZnO. Therefore, G-ZnO photocatalyst exhibited higher MB degradation.

Fig.8

Fig.9 shows the performance of several G-ZnO-CTAB catalysts prepared at different GO and Zn ratio. As shown, no significant difference in activity of MB photodegradation was observed. Much higher GO loading could slightly reduce the catalytic activity of G-ZnO-CTAB. GO can strongly absorb light for heat transformation and reduce light absorption on ZnO, resulting in lower catalytic activity of the composite.

Fig.9

To test the stability of photocatalysts, G-ZnO was collected after the first-run reaction and washed with water. Fig.10 shows a comparison of the recycled G-ZnO in the first- and second-run tests. The recycled G-ZnO still exhibited some adsorption to MB and reached equilibrium at 60 min. When light was on, MB degradation was observed and 100% MB degradation could be obtained at 200 min. Compared with the performance in the first run, G-ZnO presented slightly lower activity, which can be ascribed to intermediate poison to composite surface. The intermediates from MB degradation could be adsorbed on G-ZnO surface, making low light absorption and electron transfer for photocatalysis.

Fig.10

4. Conclusion

A one-step hydrothermal method has been successfully adopted to synthesize rGO-ZnO composites with high photocatalytic performance under UV-visible light. Zn powder could be employed and simultaneously act as a reducing agent for GO reduction and a Zn-source for ZnO formation. The use of a surfactant will promote the reduction of GO and dispersion. rGO-ZnO catalysts presented higher MB decomposition under UV-visible light than ZnO. The G-ZnO catalyst exhibited the best efficiency in MB degradation due to the mixed phase of GO and rGO, resulting in a lower band gap energy, faster electron transfer, and higher MB adsorption.

Appendix A. Supplementary material

Supplementary data (i.e., Supplementary materials for TEM images and N_2 adsorption/desorption isotherms) associated with this article can be found, in the online version, at http://

References

[1] Q. Xiang, J. Yu, M. Jaroniec, Graphene-based semiconductor photocatalysts, Chemical Society reviews, 41 (2012) 782-796.

[2] R. Leary, A. Westwood, Carbonaceous nanomaterials for the enhancement of TiO_2 photocatalysis, Carbon, 49 (2011) 741-772.

[3] P.V. Kamat, Graphene-based nanoarchitectures. Anchoring semiconductor and metal nanoparticles on a two-dimensional carbon support, The Journal of Physical Chemistry Letters, 1 (2010) 520-527.

[4] C. Gómez-Navarro, R.T. Weitz, A.M. Bittner, M. Scolari, A. Mews, M. Burghard, K. Kern, Electronic transport properties of individual chemically reduced graphene oxide sheets, Nano Letters, 7 (2007) 3499-3503.

[5] G. Eda, G. Fanchini, M. Chhowalla, Large-area ultrathin films of reduced graphene oxide as a transparent and flexible electronic material, Nat Nano, 3 (2008) 270-274.

[6] S. Stankovich, D.A. Dikin, R.D. Piner, K.A. Kohlhaas, A. Kleinhammes, Y. Jia, Yue Wu, S.T. Nguyen, R.S. Ruoff, Synthesis of graphene-based nanosheets via chemical reduction of exfoliated graphite oxide, Carbon, 45 (2007) 1558-1565.

[7] D. Luo, G. Zhang, J. Liu, X. Sun, Evaluation criteria for reduced graphene oxide, The Journal of Physical Chemistry C, 115 (2011) 11327-11335.

[8] Z.-S. Wu, W. Ren, L. Gao, B. Liu, C. Jiang, H.-M. Cheng, Synthesis of high-quality graphene with a pre-determined number of layers, Carbon, 47 (2009) 493-499.

[9] X. Mei, J. Ouyang, Ultrasonication-assisted ultrafast reduction of graphene oxide by zinc powder at room temperature, Carbon, 49 (2011) 5389-5397.

[10] S. Park, R.S. Ruoff, Chemical methods for the production of graphenes, Nat Nano, 5 (2010) 309-309.

[11] H. Sun, S. Wang, H.M. Ang, M.O. Tadé, Q. Li, Halogen element modified titanium dioxide for visible light photocatalysis, Chemical Engineering Journal, 162 (2010) 437-447.

[12] S. Liu, H. Sun, S. Liu, S. Wang, Graphene facilitated visible light photodegradation of methylene blue over titanium dioxide photocatalysts, Chemical Engineering Journal, 214 (2013) 298-303.

[13] J. Wu, X. Shen, L. Jiang, K. Wang, K. Chen, Solvothermal synthesis and characterization of sandwich-like graphene/ZnO nanocomposites, Applied Surface Science, 256 (2010) 2826-2830.

[14] B. Li, T. Liu, Y. Wang, Z. Wang, ZnO/graphene-oxide nanocomposite with remarkably enhanced visible-light-driven photocatalytic performance, Journal of Colloid and Interface Science, 377 (2012) 114-121.

[15] G. Williams, P.V. Kamat, Graphene− semiconductor nanocomposites: excited-state interactions between zno nanoparticles and graphene oxide, Langmuir, 25 (2009) 13869-13873.

[16] T. Xu, L. Zhang, H. Cheng, Y. Zhu, Significantly enhanced photocatalytic performance of ZnO via graphene hybridization and the mechanism study, Applied Catalysis B: Environmental, 101 (2011) 382-387.

[17] P.R. Shukla, S. Wang, H.M. Ang, M.O. Tadé, Photocatalytic oxidation of phenolic compounds using zinc oxide and sulphate radicals under artificial solar light, Separation and Purification Technology, 70 (2010) 338-344.

[18] H. Zhang, X. Lv, Y. Li, Y. Wang, J. Li, P25-graphene composite as a high performance photocatalyst, ACS Nano, 4 (2010) 380-386.

[19] O. Akhavan, Graphene Nanomesh by ZnO Nanorod Photocatalysts, ACS Nano, 4 (2010) 4174-4180.

[20] Y. Fan, H.-T. Lu, J.-H. Liu, C.-P. Yang, Q.-S. Jing, Y.-X. Zhang, X.-K. Yang, K.-J. Huang, Hydrothermal preparation and electrochemical sensing properties of TiO_2-graphene nanocomposite, Colloids and Surfaces B: Biointerfaces, 83 (2011) 78-82.

[21] O. Akhavan, Photocatalytic reduction of graphene oxides hybridized by ZnO nanoparticles in ethanol, Carbon, 49 (2011) 11-18.

[22] D. Fu, G. Han, Y. Chang, J. Dong, The synthesis and properties of ZnO–graphene nano hybrid for photodegradation of organic pollutant in water, Materials Chemistry and Physics, 132 (2012) 673-681.

[23] Z.J. Fan, W. Kai, J. Yan, T. Wei, L.-J. Zhi, J. Feng, Y.-m. Ren, L.-P. Song, F. Wei, Facile synthesis of graphene nanosheets via Fe reduction of exfoliated graphite oxide, ACS Nano, 5 (2011) 191-198.

[24] G. Wang, X. Shen, B. Wang, J. Yao, J. Park, Synthesis and characterisation of hydrophilic and organophilic graphene nanosheets, Carbon, 47 (2009) 1359-1364.

[25] H. Nishizawa, T. Tani, K. Matsuoka, Crystal Growth of ZnO by Hydrothermal Decomposition of Zn-EDTA, Journal of the American Ceramic Society, 67 (1984) C-98-C-100.
[26] X.M. Sun, X. Chen, Z.X. Deng, Y.D. Li, A CTAB-assisted hydrothermal orientation growth of ZnO nanorods, Materials Chemistry and Physics, 78 (2003) 99-104.
[27] W.S. Hummers Jr, Hummers, Preparation of graphitic oxide, Journal of the American Chemical Society, 80 (1958) 1339-1340.
[28] J.Y. Jang, M.S. Kim, H.M. Jeong, C.M. Shin, Graphite oxide/poly(methyl methacrylate) nanocomposites prepared by a novel method utilizing macroazoinitiator, Composites Science and Technology, 69 (2009) 186-191.
[29] H. Zhang, D. Yang, Y. Ji, X. Ma, J. Xu, D. Que, Low Temperature Synthesis of Flowerlike ZnO Nanostructures by Cetyltrimethylammonium Bromide-Assisted Hydrothermal Process, The Journal of Physical Chemistry B, 108 (2004) 3955-3958.
[30] N. Li, G. Liu, C. Zhen, F. Li, L. Zhang, H.-M. Cheng, Battery performance and photocatalytic activity of mesoporous anatase TiO_2 nanospheres/graphene composites by template-free self-assembly, Advanced Fnctional Materials, 21 (2011) 1717-1722.
[31] M. Khenfouch, M. Baïtoul, M. Maaza, White photoluminescence from a grown ZnO nanorods/graphene hybrid nanostructure, Optical Materials, 34 (2012) 1320-1326.
[32] A.C. Ferrari, J.C. Meyer, V. Scardaci, C. Casiraghi, M. Lazzeri, F. Mauri, S. Piscanec, D. Jiang, K.S. Novoselov, S. Roth, A.K. Geim, Raman spectrum of graphene and graphene layers, Physical Review Letters, 97 (2006) 187401.
[33] Q.-P. Luo, X.-Y. Yu, B.-X. Lei, H.-Y. Chen, D.-B. Kuang, C.-Y. Su, Reduced graphene oxide-hierarchical ZnO hollow sphere composites with enhanced photocurrent and photocatalytic activity, The Journal of Physical Chemistry. C, 116 (2012) 8111-8117.
[34] S. Zhu, J. Zhang, X. Liu, B. Li, X. Wang, S. Tang, Q. Meng, Y. Li, C. Shi, R. Hu, B. Yang, Graphene quantum dots with controllable surface oxidation, tunable fluorescence and up-conversion emission, RSC Advances, 2 (2012) 2717-2720.
[35] X. Zhou, T. Shia, H. Zhou, Hydrothermal preparation of ZnO-reduced graphene oxide hybrid with high performance in photocatalytic degradation, Applied surface science, 258 (2012) 6204-6211.
[36] A. Eckmann, A. Felten, A. Mishchenko, L. Britnell, R. Krupke, K.S. Novoselov, C. Casiraghi, Probing the nature of defects in graphene by raman spectroscopy, Nano Letters, 12 (2012) 3925-3930.

[37] Z. Ni, Y. Wang, T. Yu, Z. Shen, Raman spectroscopy and imaging of graphene, Nano Research, 1 (2008) 273-291.
[38] U. Alver, W. Zhou, A.B. Belay, R. Krueger, K.O. Davis, N.S. Hickman, Optical and structural properties of ZnO nanorods grown on graphene oxide and reduced graphene oxide film by hydrothermal method, Applied Surface Science, 258 (2012) 3109-3114.
[39] L. Jia, D.-H. Wang, Y.-X. Huang, A.-W. Xu, H.-Q. Yu, Highly durable N-doped graphene/CdS nanocomposites with enhanced photocatalytic hydrogen evolution from water under visible light irradiation, The Journal of Physical Chemistry. C, 115 (2011) 11466-11473.
[40] Z. Gu, C. Li, G. Wang, L. Zhang, X. Li, W. Wang, S. Jin, Synthesis and characterization of polypyrrole/graphite oxide composite by in situ emulsion polymerization, Journal of Polymer Science Part B: Polymer Physics, 48 (2010) 1329-1335.
[41] S. Wang, H. Sun, H.M. Ang, M.O. Tadé, Adsorptive remediation of environmental pollutants using novel graphene-based nanomaterials, Chemical Engineering Journal, 226 (2013) 336-347.
[42] H. Sun, S. Liu, S. Liu, S. Wang, A comparative study of reduced graphene oxide modified TiO_2, ZnO and Ta_2O_5 in visible light photocatalytic/photochemical oxidation of methylene blue, Applied Catalysis B: Environmental, DOI: 10.1016/j.apcatb.2013.03.027 (2013).
[43] Y. Yokomizo, S. Krishnamurthy, P.V. Kamat, Photoinduced electron charge and discharge of graphene–ZnO nanoparticle assembly, Catalysis Today, 199 (2013) 36-41.
[44] H. Fan, X. Zhao, J. Yang, X. Shan, L. Yang, Y. Zhang, X. Li, M. Gao, ZnO–graphene composite for photocatalytic degradation of methylene blue dye, Catalysis Communications, 29 (2012) 29-34.
[45] B. Li, H. Cao, ZnO@graphene composite with enhanced performance for the removal of dye from water, Journal of Materials Chemistry, 21 (2011) 3346-3349.
[46] N. Yang, J. Zhai, D. Wang, Y. Chen, L. Jiang, Two-dimensional graphene bridges enhanced photoinduced charge transport in dye-sensitized solar cells, ACS Nano, 4 (2010) 887-894.

List of Figures

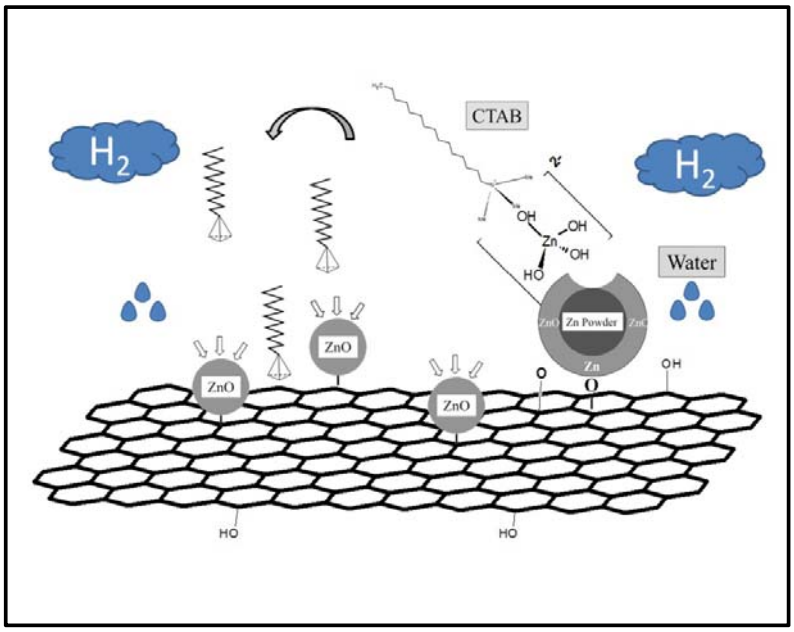

Fig.1 Synthesis of G-ZnO-CTAB composite.

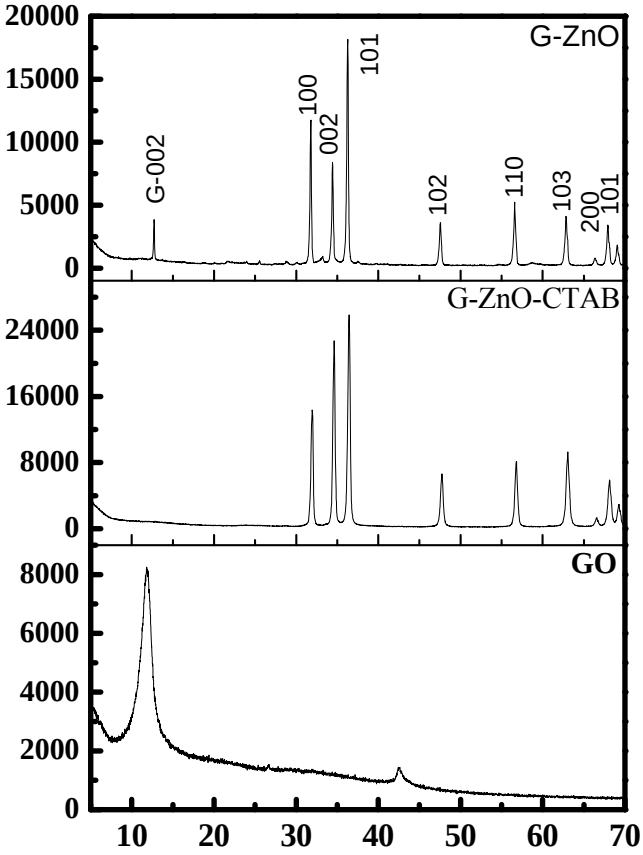

Fig. 2. XRD patterns of GO, G-ZnO, and G-ZnO-CTAB samples.

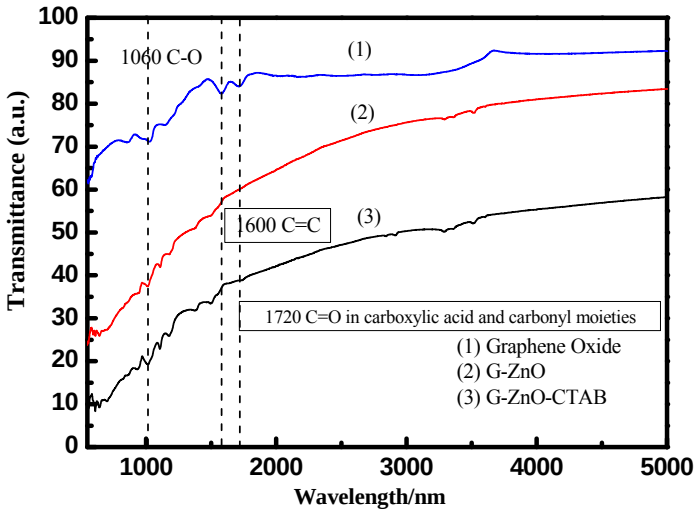

Fig. 3 FTIR spectra of GO, G-ZnO, G-ZnO-CTAB.

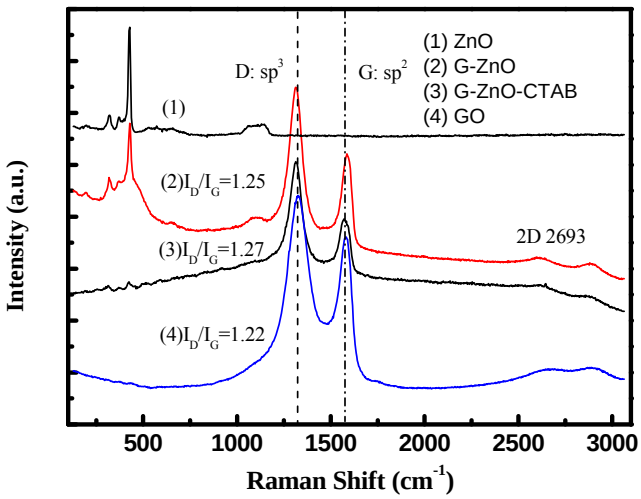

Fig. 4. Raman spectra of GO, G-ZnO-CTAB, G-ZnO samples.

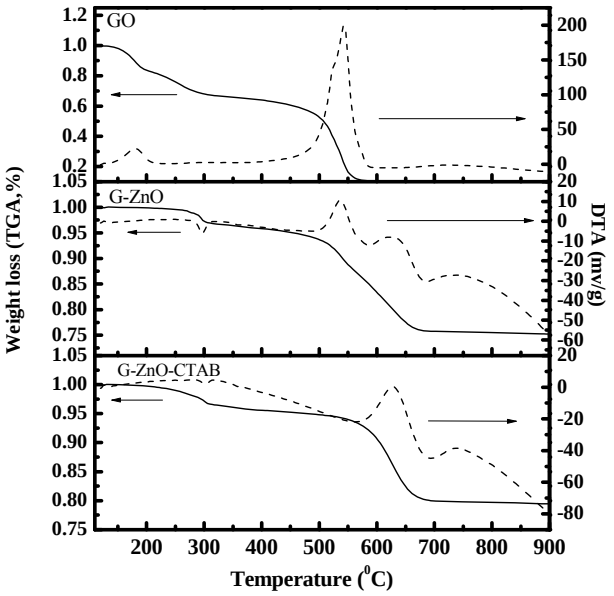

Fig. 5 TG-DTA profiles of GO, G-ZnO, G-ZnO-CTAB samples.

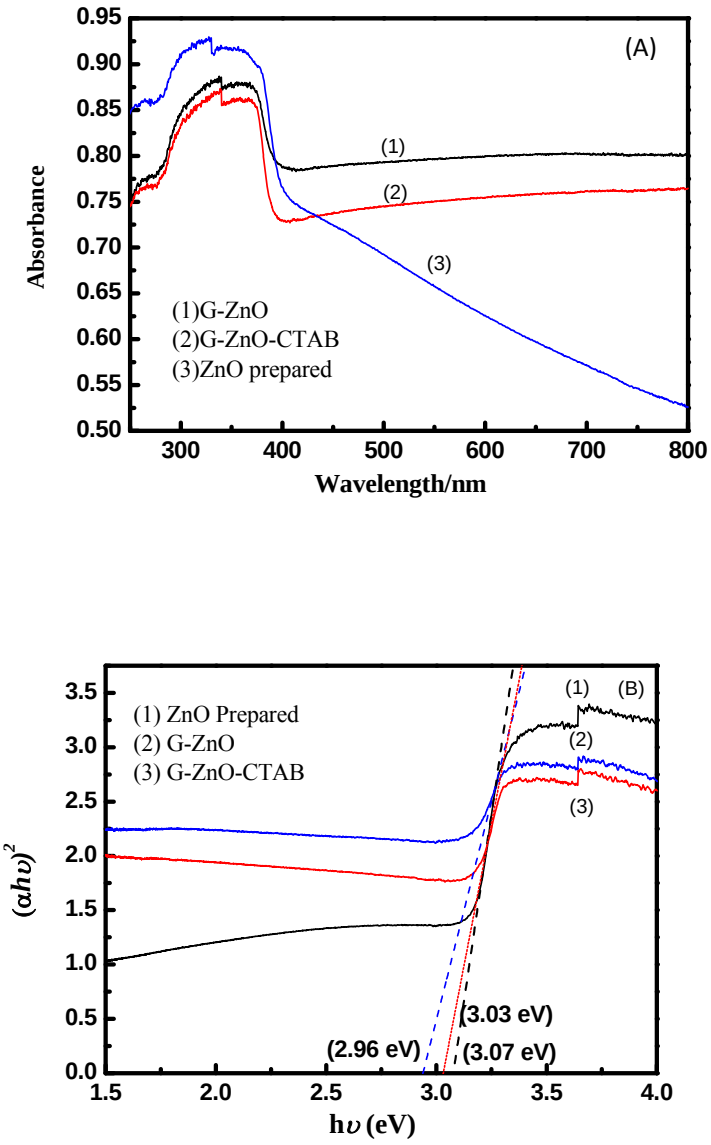

Fig. 6. UV-vis diffuse reflectance spectra (A) and the $(ah\upsilon)^2$ vs $h\upsilon$ graph (B) of ZnO , G-ZnO, G-ZnO-CTAB .

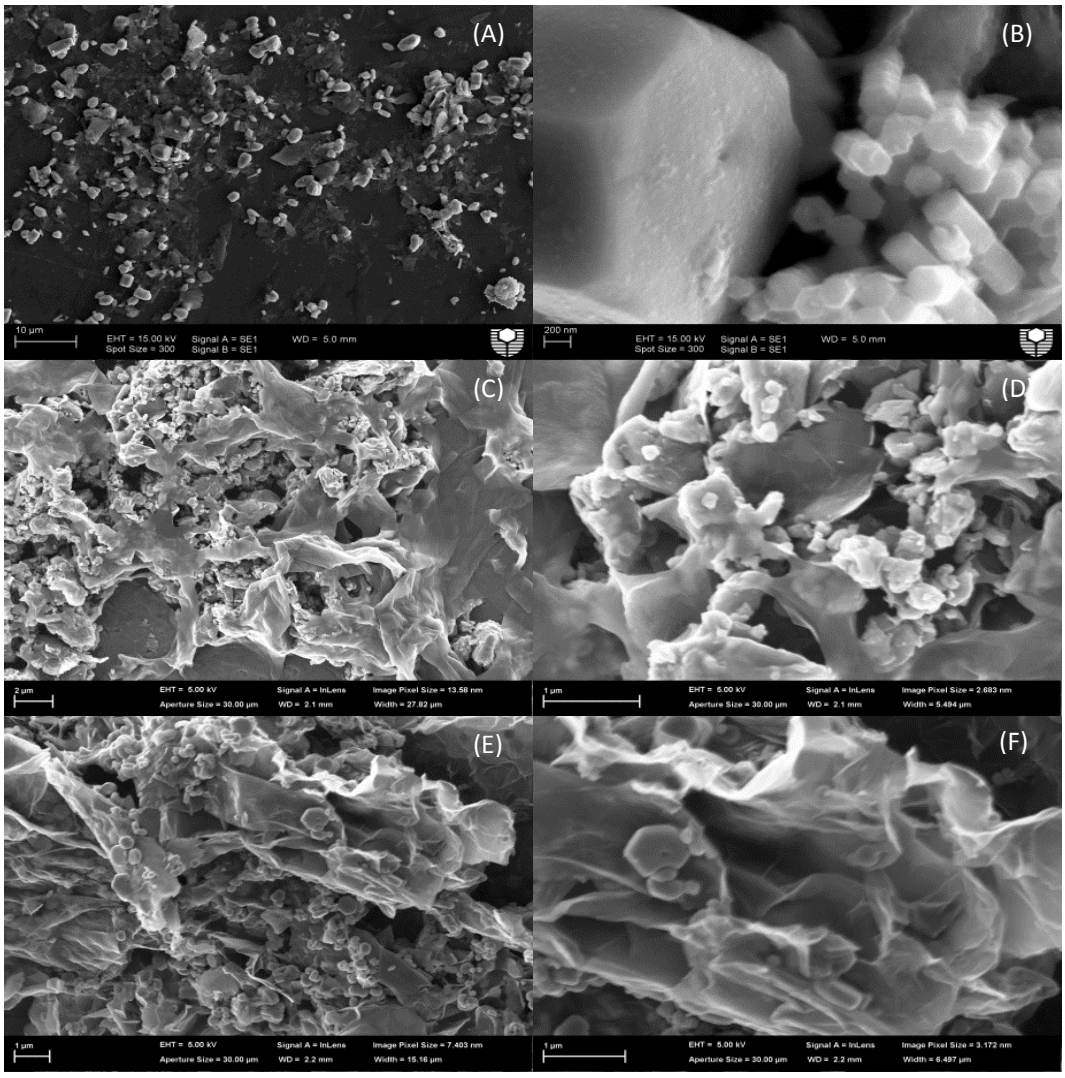

Fig. 7. SEM images of ZnO prepared (A, B), G-ZnO (C, D), and G-ZnO-CTAB (E, F).

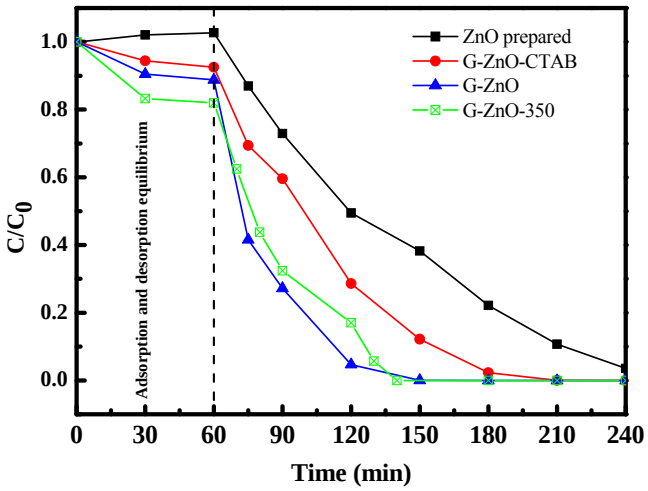

Fig. 8. Photodegradation of methylene blue solutions under solar irradiations.

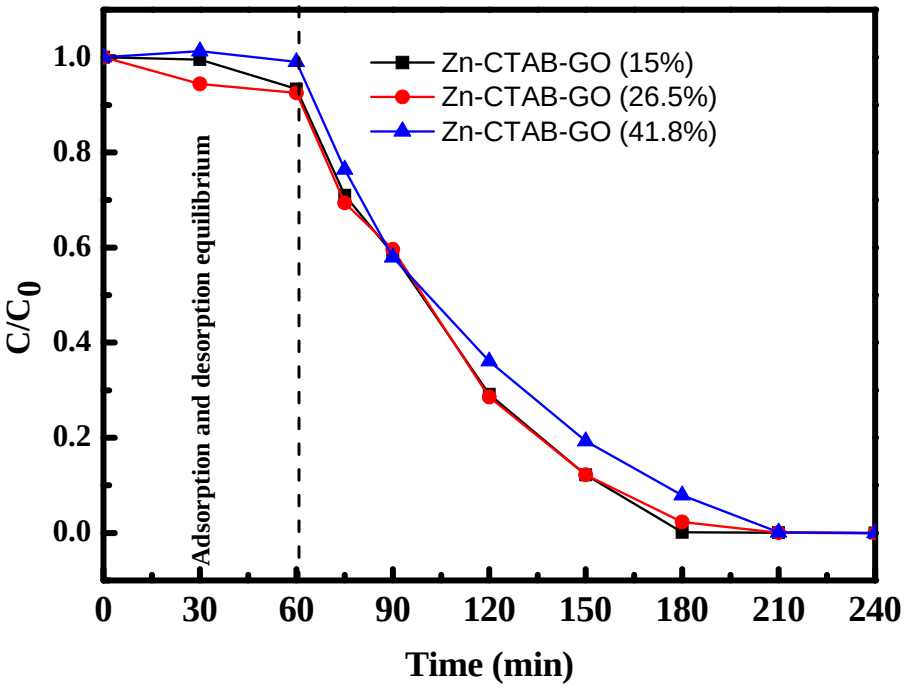

Fig. 9. Photodegradation of methylene blue solutions under solar irradiations at varying Zn/GO ratios.

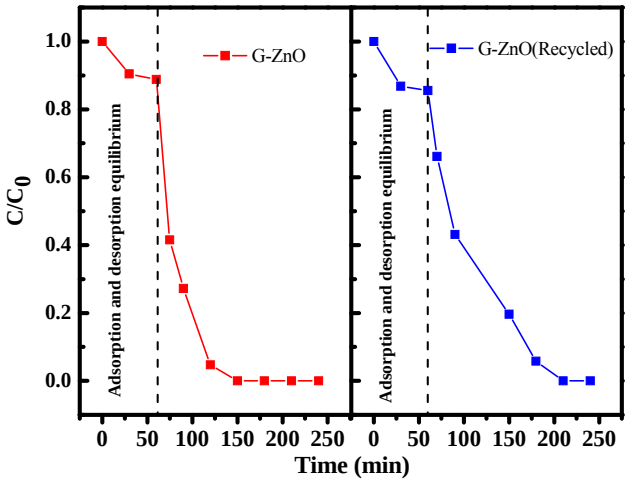

Fig. 10. Photodegradation of methylene blue solutions under solar irradiations in recycled runs.